A Compact, Capacitively-Fed UWB Antenna With Monopole-Like Radiation Characteristics

Mingjian Li, *Member, IEEE,* and Nader Behdad, *Fellow, IEEE*

***Abstract*—A compact, ultra-wideband (UWB) antenna occupying a cylindrical volume and providing omni-directional monopole-like radiation is introduced. The antenna consists of two closely-placed three-dimensional (3D) loops, two parasitic small loops, and a circular top hat. Two strip-shaped probes, each coupling with one loop, are used to feed the antenna in common mode. UWB operation is achieved by taking advantage of the magnetic coupling of the parallel-fed 3D loops. Small electrical dimensions of the antenna are due to the special capacitive proximity feeding scheme and the presence of the top hat. A prototype with 4.1:1 bandwidth is designed, fabricated, and characterized. The antenna demonstrates a VSWR better than 2:1 and monopole-like omni-directional radiation characteristics across this entire band. It occupies a cylindrical volume with a diameter of 0.14λ_{min} and a height of 0.09λ_{min}, where λ_{min} is the free-space wavelength at the lowest frequency of operation. The antenna has a $k_{min}a = 0.73$, where k_{min} is the wavenumber at its lowest frequency of operation. The fabricated prototype is demonstrated to have a lowest frequency of operation that is only 10% above the theoretical limits on UWB antennas. Further miniaturization of the antenna using a spherical top hat is also examined and demonstrated to be capable of reducing $k_{min}a$ values down to 0.60.**

***Index Terms*—Broadband antennas, electrically small antennas, ultrawideband antennas, omnidirectional antennas.**

I. Introduction

ULTRAWIDEBAND (UWB) technology has many applications in wireless communications and sensing systems ranging from ground penetrating radars and high data rate short-range wireless networks to civilian and military communications systems [1]. UWB antennas are critical parts of any UWB wireless systems. The design of a UWB antenna becomes very challenging for systems operating at the lower RF/microwave frequencies. This is due to the fact that the wavelength is very large at these frequencies and generally having physically large antennas is not desirable due to space limitations. This problem is particularly severe in military communications systems that operate at HF, VHF, and UHF bands because in such applications, having antennas with low visual signatures is of paramount importance. Such antennas are generally required to radiate vertically-polarized waves with omni-directional radiation patterns similar to a monopole antenna. The current antennas of choice for these applications tend to be monopole whip antennas used in conjunction with automatic impedance tuners [2]. These antennas, however, suffer from two major drawbacks. The first drawback is the relatively large heights of a conventional monopole whip antenna. When mounted on a vehicle, such an antenna significantly protrudes from the top surface of the vehicle drastically increasing the visual signature of the vehicle. The second issue with monopole whip antennas is their narrow bandwidths which limits the types of waveforms that they can receive or transmit. Therefore, development of compact, low-profile, and ultra-wideband antennas is of particular interest in many communications systems that operate at HF, VHF, and UHF frequencies.

In the past several decades, considerable efforts have been devoted to conducting research on investigating the fundamental limitations of electrically-small antennas as well as designing antennas providing performance levels close to these fundamental limitations. Since Wheeler [3] and Chu [4] derived the well-known theoretical limits on the performances of electrically-small antennas, a number of designs have been reported that approach these fundamental limits. A rather comprehensive survey of these antennas is provided in [5], where the performances of the most promising designs in this area are compared against the theoretical limits derived by Chu. Several specific examples of innovative designs for small antennas whose performances are compared in [5] include linear helix [6], spherical electric [7] and magnetic [8] dipoles, dual-mode spherical dipoles [9], miniaturized monopoles [10], [11], metamaterial inspired [12], and dielectric resonator [13] antennas. Among these antennas, the spherical electric and magnetic dipole antennas have performance levels that nearly approach the fundamental limits predicted by Chu. However, the bandwidth provided by these antennas is still not sufficient to meet the stringent demands of many UWB systems.

To increase the bandwidth of monopole-type radiators, a number of different techniques have been examined. A variety of printed monopole antennas that provide UWB operation in a planar form factor are examined in the 3.1-10.6 GHz band [14]–[16]. However, at its lowest frequency of operation, a printed monopole tends to have relatively large dimensions. Specifically, most printed monopole antennas have $k_{min}a$ values larger than 1, where k_{min} is the wavenumber at the lowest frequency of operation of the antenna and a is the radius of the smallest sphere that circumscribes the antenna. Thus scaling these designs to HF-UHF frequencies results

This material is based upon work supported by the Office of Naval Research under ONR Award No. N00014-15-1-2207 and Award No. N00014-16-1-2098. The authors are with the Department of Electrical and Computer Engineering, University of Wisconsin-Madison, Madison, WI, 53706 USA (e-mail: mli454@wisc.edu and behdad@wisc.edu)

This article has been accepted for publication in a future issue of this journal, but has not been fully edited. Content may change prior to final publication. Citation information: DOI 10.1109/TAP.2016.2641925, IEEE Transactions on Antennas and Propagation

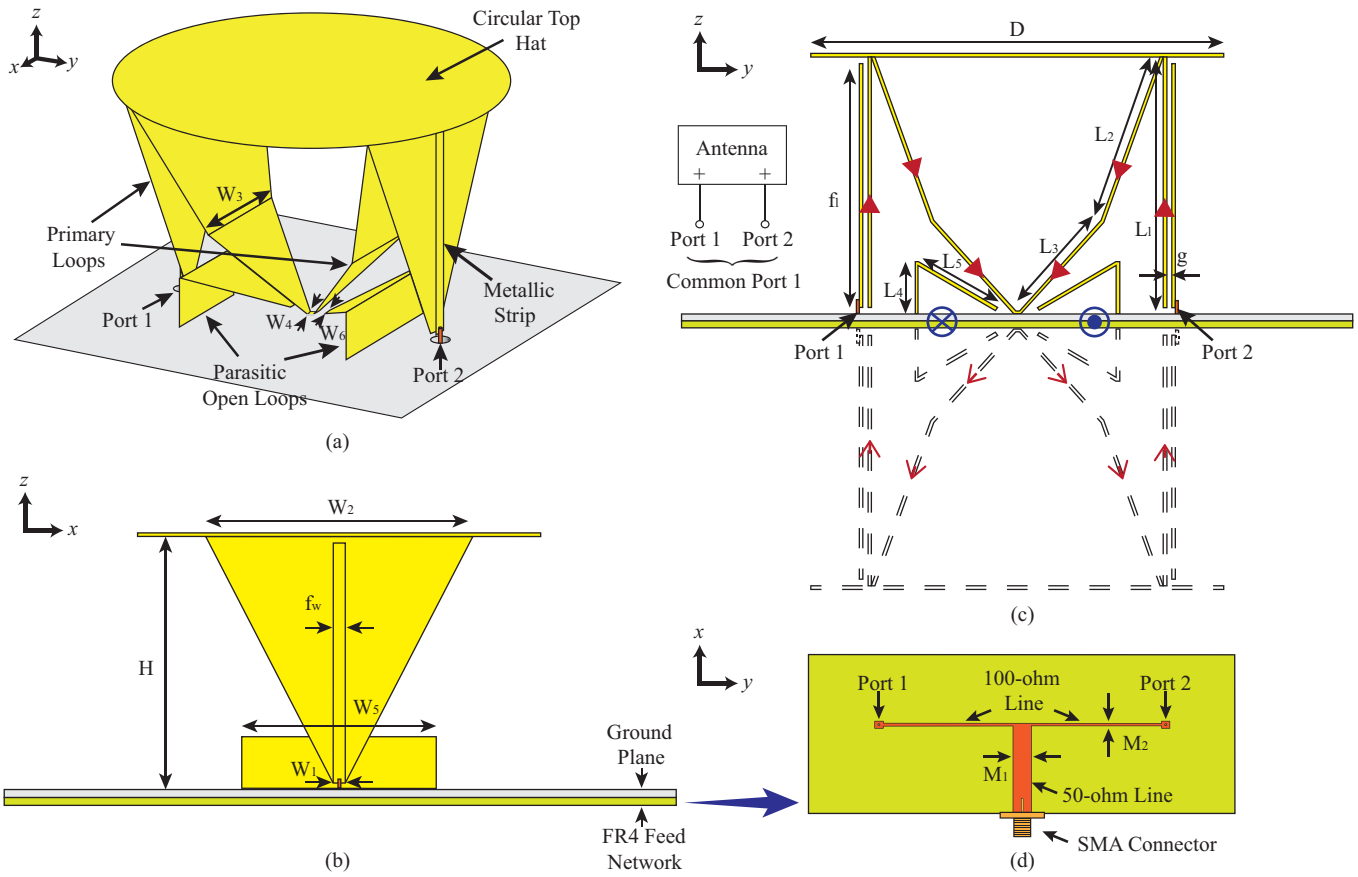

Fig. 1. Topology of the proposed antenna. (a) 3-D view. (b) Side view in the $x-z$ plane. (c) Side view in the $y-z$ plane. (d) View of the bottom side of the ground plane showing the feed network of the antenna fabricated on an FR4 substrate.

in structures with larger than desirable physical dimensions. Multi-resonant structures have also been investigated for bandwidth enhancement of small antennas. One of the earliest examples of such structures is the antenna invented by Goubau [17]. This structure occupied a cylindrical volume with a diameter of $0.14\lambda_{min}$ and a height of $0.09\lambda_{min}$ resulting in a $k_{min}a = 0.73$. Subsequently, other versions of this antenna were reported by Friedman [18] and other antenna designers [19], [20]. The designs presented in [17]–[20] can provide wideband response in a compact volume. However, the bandwidths of these antennas are limited to about one octave. More recently, several antennas were investigated for their very wide impedance bandwidths [21]–[29]. Among them, a low-profile UWB antenna with monopole-like radiation characteristics was reported in [28]. This antenna consists of two diamond-shaped loops and a rectangular top hat and exhibits more than two octaves of bandwidth. Subsequently, modifications were made to this antenna to further increase its bandwidth [29]. One of the main attractive features of the antennas reported in [28], [29] is their extremely small heights compared to the wavelength. However, this comes at the expense of increased lateral dimensions. Consequently, for the lowest frequency of operation that these antennas offer, they have larger maximum linear dimensions compared to the Goubau antenna for example (i.e., the $k_{min}a$ values of the antennas reported in [28], [29] are 1.09 and 1.19 respectively whereas that of the Goubau antenna is 0.73).

In this paper, we present a new type of small, ultra-wideband antenna. At its lowest frequency of operation, this antenna has a $k_{min}a = 0.73$, which is the same as that of the Goubau antenna. However, it provides a significantly wider **bandwidth of more than two octaves (4.1:1)**. The proposed antenna occupies a cylindrical volume with a radius of $R = 0.072\lambda_{min}$ and a height of $H = 0.09\lambda_{min}$. A prototype of the proposed antenna is designed, fabricated, and experimentally characterized. The fabricated prototype is shown to operate over the frequency band of 0.69-2.84 GHz with monopole-like omni-directional radiation patterns and a VSWR better than 2:1. The performance of this antenna is also compared against the Sohl-Gustafsson theoretical limits on the performances of UWB antennas [30]. It is demonstrated that the proposed design is a nearly optimum design, operating to **within 10% of the theoretical limitations**. We also report a version of this antenna with a spherical form factor in which the lowest frequency of operation of the design is further reduced without increasing its maximum linear dimension resulting in **reduction of the $k_{min}a$ value of the antenna down to 0.6**. To the best of our knowledge, this is the lowest reported $k_{min}a$ of any monopole-type, ultrawideband antenna reported to date.

This article has been accepted for publication in a future issue of this journal, but has not been fully edited. Content may change prior to final publication. Citation information: DOI 10.1109/TAP.2016.2641925, IEEE Transactions on Antennas and Propagation

II. Antenna Description and Principles of Operation

Fig. 1(a) shows the three-dimensional (3-D) view of the proposed antenna. The structure is composed of two primary 3D loops each split with a series distributed capacitor, two parasitic open loops, and a circular top hat. The primary loops have their inner ends shorted to the ground plane and their outer edges open circuited. The small, parasitic loops have their outer edges short circuited to the ground plane and their inner edges are left open circuited. Together with the top hat, the small loops are used to improve the impedance matching and reduce the lowest operating frequency. Two metallic strip-shaped probes located on the outside of loops are used to feed the antenna with a distributed capacitive coupling arrangement. The feed points are labeled as Ports 1 and 2. The proximity coupled feeds help with reducing the lowest frequency of operation of the antenna by introducing a series capacitance in line with the feed. The antenna is fed in the common mode by exciting Ports 1 and 2 with signals having the same magnitudes and phases.

Fig. 1(b) shows the side view of the antenna in the $x-z$ plane. The proposed antenna is mounted on a ground plane with dimensions of 430 mm $\times$ 430 mm. Most of the simulations conducted in this work assume an infinite ground plane size primarily to reduce the simulation time. In practice, however, the ground plane cannot be infinite but should be large enough to ensure that the antenna performance is not affected drastically. On the bottom side of the ground plane, a thin dielectric substrate with small dimensions of 70 $mm \times 70$ mm is placed (FR4 with ε = 4.4 and thickness = 1.58 mm).

Fig. 1(c) shows the side view of the antenna in the $y-z$ plane. The impact of the infinite ground plane can easily be taken into account by examining the image of the active parts of the antenna (shown with dashed lines in Fig. 1(c)). The primary half loops together with their images construct two full loops split with two distributed capacitors, which are placed very closely and excited in parallel. These split loops are strongly coupled with each other. As can be seen, the excited currents on the two loops are in the same direction and mirror image of each other. The currents flowing in each loop generate equivalent magnetic currents along the directions shown in Fig. 1(c). However, the excited equivalent magnetic currents at the center of the loops are oppositely directed resulting in strong mutual coupling between the two loops.

A common-driven antenna with two ports can be regarded as a single-ended two-port network as shown in the inset of Fig. 1(c). The two ports fed together in parallel can be designated as a Common Port 1. Thus, the common-to-common reflection coefficient of the Common Port 1 (S_{cc11}) is defined as [31],

$$S_{cc11} = \frac{1}{2}(S_{11} + S_{12} + S_{21} + S_{22}). \quad (1)$$

If the antenna is a symmetrical structure and a reciprocal network, then $S_{11} = S_{22}$ and $S_{12} = S_{21}$, and therefore (1) can be rewritten as,

$$S_{cc11} = S_{11} + S_{12}, \quad (2)$$

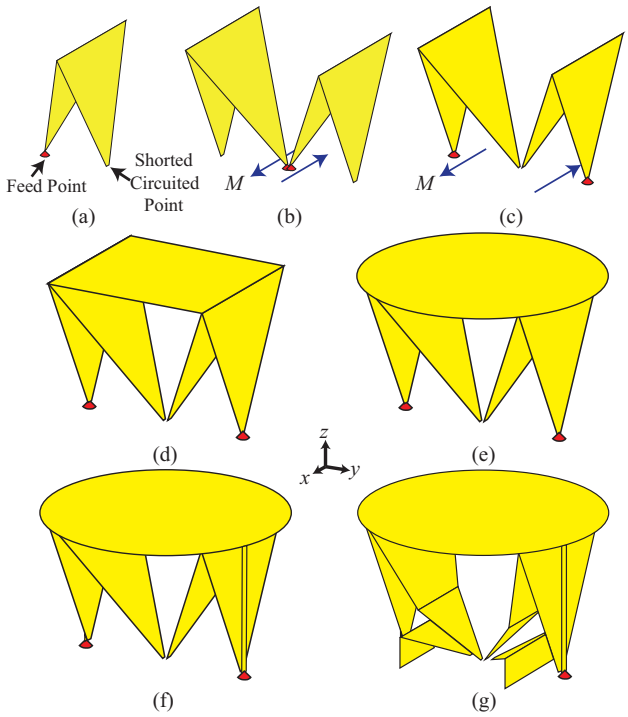

Fig. 2. Various stages of evolution of the proposed antenna. (a) A single loop with 3D surface. (b) Center-fed twin coupled loops. (c) Outer-fed twin coupled loops. (d) Outer-fed twin coupled loops with a rectangular top hat. (e) Outer-fed twin coupled loops with a circular top hat. (f) Capacitively-fed twin coupled loops with a circular top hat. (g) Final design utilizing two parasitic smaller loops for improved impedance matching.

Hence, the mutual coupling between the two ports (S_{12}) can be used as a means to reduce the spectral variations of the self impedance of each loop. In other words, if the spectral variations of S_{11} and S_{12} cancel each other, a wideband impedance match at the common port 1 can be obtained [32]. This is done primarily by shaping the primary loops through controlling the folding and slanting of the arms. Additionally, the placement of a pair of parasitic, open small loops inside the main loops is used as an additional tuning mechanism to improve the impedance matching of the antenna towards the band edges.

Fig. 1(d) shows the microstrip feed network printed on the FR4 substrate placed underneath the ground plane of the antenna. The input signal is fed into a 50 Ω line from an SMA connector and split between two microstrip line branches each with a 100 Ω characteristic impedance through a microstrip T-junction. Thus, the antenna should be designed to have an input impedance of $\sim$100 Ω at each of the two input ports. This way, the antenna can be matched well to the two output branches of the feed network.

III. Design Process and Guidelines

Fig. 2 shows the different stages of evolution that resulted in the antenna proposed in this work. Comparison of these seven different stages of the development of the antenna reveals the role of each significant part of the structure in obtaining the desired UWB response. In the following sub-sections, we will present full-wave simulation results that describe the role of

This article has been accepted for publication in a future issue of this journal, but has not been fully edited. Content may change prior to final publication. Citation information: DOI 10.1109/TAP.2016.2641925, IEEE Transactions on Antennas and Propagation

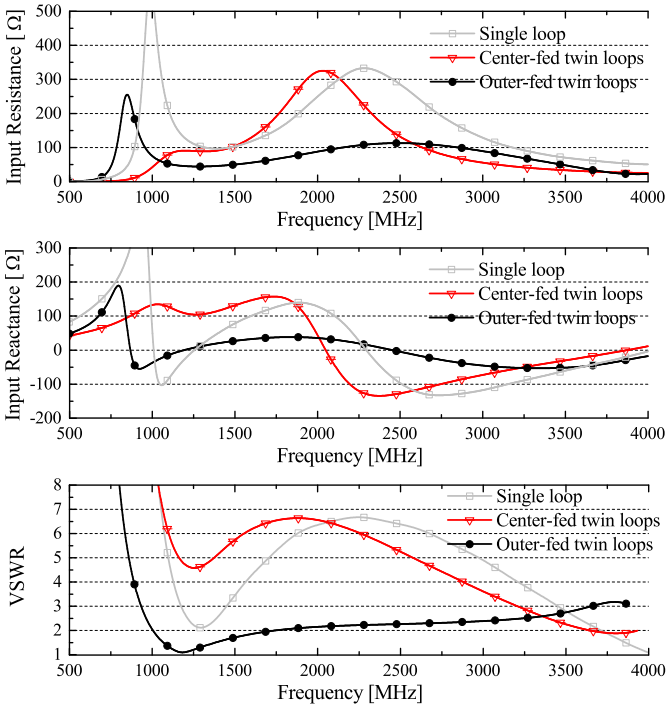

Fig. 3. Simulated input resistances, input reactances, and VSWRs of the single loop, the center-fed twin coupled loop, and the outer-fed twin coupled loop antennas shown in Figs. 2(a)-2(c).

each part of the structure. All simulations were done using the time domain solver of CST Microwave Studio. The response of the antenna (i.e., S_{cc11}, $VSWR_{cc}$, and Z_{cc11}), is obtained by combining the S-parameters of the two-port antenna shown in Fig. 1 using an ideal power splitter modeled in CST.

A. Twin Loops

The design of the antenna starts from the structure shown in Fig. 2(a). This antenna is a single loop (or folded monopole) antenna including two metallic plates. One of these plates is slanted and short-circuited to the ground while the other is vertically placed and has one end as the feed point. The input impedance of this antenna as well as its VSWR are shown in Fig. 3. Observe that the antenna barely shows a VSWR of 2 at around 1.3 GHz and does not offer a wideband impedance match. However, examination of the resistance and reactance of the single loop reveals that, while impedance mismatched, the resonances of this loop are not very high Q. Therefore, this structure has the potential of providing wideband impedance match if an appropriate impedance matching technique is used.

To improve the impedance matching of the antenna, two identical single loops of the type shown in Fig. 2(a) are used in the arrangement shown in Fig. 2(b). The feed points are located at the inner positions of the loops. The input impedance of this antenna as well as its input VSWR are also shown in Fig. 3. In this structure, the two ports are fed in the common mode and the results shown in Fig. 3 represent the common-mode input impedance and input VSWR of the system. While the impedance matching of this structure is deteriorated compared to that of the single loop case, examination of its input resistance and reactance reveals that the antenna Q at each of its resonances is lower compared to the previous case. This is primarily due to the mutual coupling between the two loops as discussed in [32]. However, due to the large antenna reactance the input VSWR of this structure is quite high. This large input reactance is due to the fact that the loops have a relatively large height to width ratio. This, combined with feeding the loops at the center, causes their oppositely directed effective magnetic dipole moments to be closer to each other as shown in Fig. 2(b) resulting in strong reactive near fields. For each loop, the equivalent effective magnetic dipole moment is closer to the feed point than the shorting point. This is verified by examining the electric current distribution on the loop arms as well as the electric and magnetic field densities in the antenna's near field.

To circumvent this problem, the feed points are moved to the outer positions of the loops and the inner positions are shorted to the ground as shown in Fig. 2(c). This change causes the oppositely-directed magnetic dipole moments of the two loops to separate apart, thereby reducing the strength of the reactive near field. This drastically reduces the input reactance of the antenna and allows for a wideband impedance match to be achieved. This change also reduces the frequency of the first parallel resonance of the antenna while slightly increasing that of the second one. As a result, the input impedance is increased below 1100 MHz and decreased in the frequency band from 1100 to 2500 MHz, creating much better conditions for improving the impedance matching of the antenna. Fig. 3 shows the input impedance of this antenna as well as its input VSWR. Observe that the quality factors of the resonances of this structure are very low and the input resistance and reactance of the antenna are rather constant over a broad frequency band. Therefore, the input VSWR of the antenna is reduced significantly and a broadband impedance match is obtained.

B. Top Hat

Using a capacitive top hat to load a monopole antenna is a classical technique for reducing its lowest frequency of operation for a given occupied volum [17], [18], [23], [25]. The top hat serves to add capacitance to the upper end of the monopole, which reduces the antenna's resonant frequency but increases its Q. In the next stage of evolution of the proposed antenna, this technique is applied, where first a rectangular top hat is added to the top of the twin loops as shown in Fig. 2(d). Fig. 4 shows the input impedance and the input VSWR of this antenna. Observe that the first resonant frequency of the loops with the rectangular top hat is shifted downwards in comparison with the loops without the top hat. This modification, however, results in increasing the in-band VSWR of the antenna. To efficiently utilize the entire cylindrical volume occupied by this antenna, the shape of the top hat is then changed to a circular one as shown in Fig. 2(e). The circular top hat has a larger coupling surface and introduces more capacitance, thereby offering further miniaturization of the antenna. This can be observed from Fig. 4 as well where it is seen that the frequency of the first series resonance

This article has been accepted for publication in a future issue of this journal, but has not been fully edited. Content may change prior to final publication. Citation information: DOI 10.1109/TAP.2016.2641925, IEEE Transactions on Antennas and Propagation

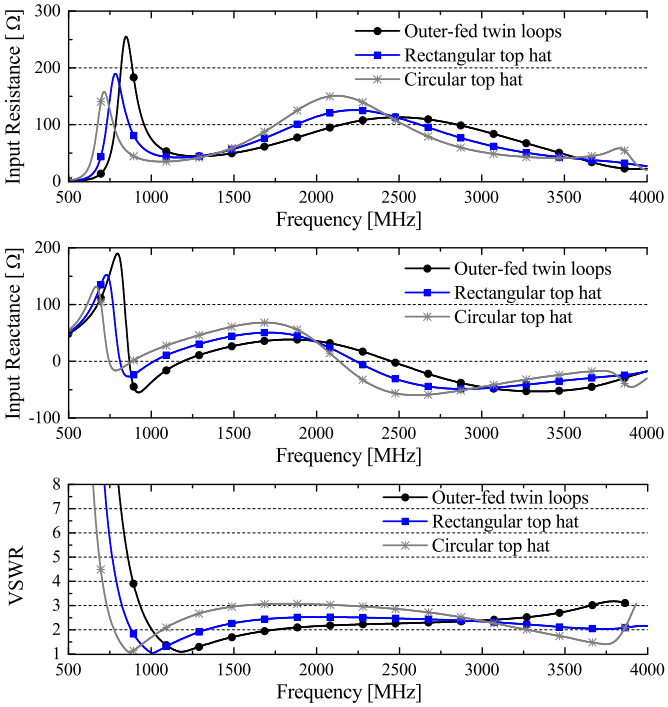

Fig. 4. Simulated input resistances, input reactances, and VSWRs of the outer-fed twin coupled loop antenna, the twin coupled loop antenna with a rectangular top hat, and the twin coupled loop antenna with a circular top hat seen in Figs. 2(c)-2(e).

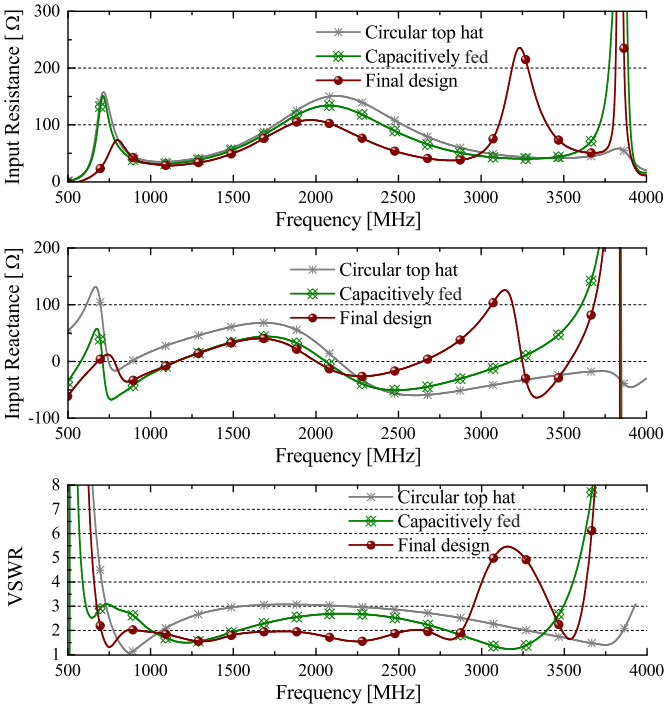

Fig. 5. Simulated input resistances, input reactances, and VSWRs of the twin coupled loop antenna with a circular top hat, the capacitively-fed twin coupled loop antenna with a circular top hat, and the final proposed antenna shown in Figs. 2(e)-2(g).

of the antenna is further reduced. However, this additional miniaturization comes at the expense of further worsening of the antenna's input VSWR in the middle of its frequency band, where the VSWR is now raised to approximately 3. Using the circular top hat instead of the rectangular one does not increase the radius of the smallest circumscribing sphere of the antenna, a (i.e., the Chu's sphere) and enables a more efficient utilization of the volume within Chu's sphere.

C. Capacitively Coupled Feeds

At this stage of the evolution, the antenna shown in Fig. 2(e) offers a wideband impedance matching and a relatively low, minimum frequency of operation. However, its in-band VSWR of 3:1 can still be improved. To accomplish this, we propose using a capacitively-coupled feed to feed the antenna. Capacitively coupled feeds are sometimes used to increase the impedance bandwidths of microstrip patch antennas [33]. In such structures, a capacitively coupled small patch or microstrip open stub is combined with the vertical feed probe to compensate the inductance introduced by the probe itself. Fig. 5 shows that the input impedance of the antenna shown in Fig. 2(e) (the twin loops with a circular top hat) is inductive in the frequency range from 500-2200 MHz. Hence, using capacitively coupled feeds can compensate for the inductance in the lower frequency band of the structure. This is accomplished by modifying the structure of the antenna as shown in Fig. 2(f). Two strip-shaped metallic probes are used as capacitively coupled feeds to feed each loop of the antenna. The input impedance and the input VSWR of this antenna are shown in Fig. 5. Observe that the input resistance of this antenna is very similar to that of the structure shown in Fig. 2(e). However, the input reactance is reduced significantly in the frequency band of 500-2300 MHz and increased above 2300 MHz where the coupled feeds turn to be inductive. Introduction of this capacitively-coupled feeding scheme introduces a series resonance with a frequency lower than that of the main parallel resonance of the loops. This allows for reducing the input reactance of the antenna at lower frequencies and further reducing the lowest frequency of operation of the structure. In this case, the lowest resonant frequency of the antenna is reduced significantly down to 580 MHz.

The introduction of the capacitively-coupled feeding scheme is effective in reducing the lowest frequency of operation of the antenna and it also slightly improves the in-band input VSWR of the structure. However, the in-band VSWR can still be further improved and reduced ideally to a level lower than 2:1. To accomplish this, the primary twin loops are deformed at the slanted portions of the loops and two parasitic loops are inserted in the volume below the bent primary loops as shown in Fig. 2(g). This modification to the antenna topology offers another degree of freedom in controlling the mutual coupling between the two loops and fine tuning the impedance matching of the antenna. Fig. 5 shows the input impedance and VSWR of this antenna. Observe that the input VSWR is reduced to a level below 2 over practically the entire frequency band of the structure. However, the lowest resonant frequency of the antenna is also shifted higher to around 680 MHz. Moreover, a strong parallel resonance is also introduced in the

This article has been accepted for publication in a future issue of this journal, but has not been fully edited. Content may change prior to final publication. Citation information: DOI 10.1109/TAP.2016.2641925, IEEE Transactions on Antennas and Propagation

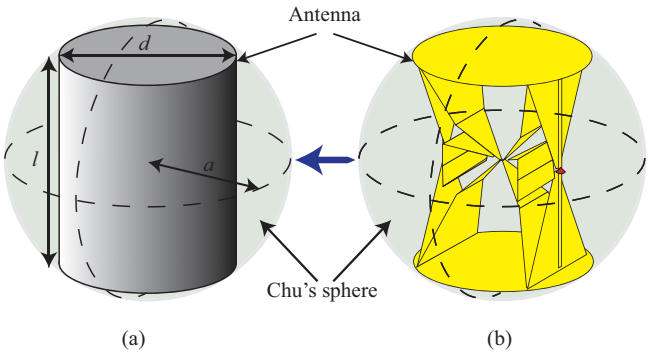

Fig. 6. (a) A general antenna occupying a cylindrical volume with a diameter of d and a height of l fitted inside the Chu sphere with a radius of a. (b) Topology of the dipole version of the proposed antenna fitted inside the Chu's sphere of radius a. The antenna occupies a cylindrical volume similar to the general structure shown in part (a).

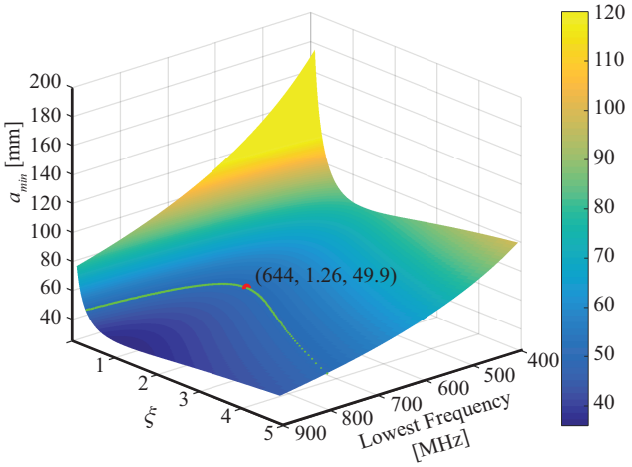

Fig. 7. The minimum required a value (a_{min}) to obtain a given combination of ξ (height-to-width ratio) and lowest frequency of operation for the generic UWB antenna discussed in Section IV-A. This generic antenna occupies the cylindrical volume shown in Fig. 6(a) and its other attributes are described in detail in Section IV-A.

vicinity of 3.25 GHz, which reduces the impedance bandwidth of the proposed antenna at higher frequencies. This is due to the fact that the parasitic loops resonate at around 3.25 GHz. Nevertheless, the design shown in Fig. 2(g) provides a decent compromise between wide bandwidth, low minimum frequency of operation, and a low VSWR below 2.

IV. Comparison of the Performance of the Proposed Antenna Against Fundamental Limits

A. Examining the Fundamental Limits

The fundamental limits on the performances of small antennas proposed by Chu [4] and investigated later on by many other researchers assume that the antenna is a single mode structure that fits within a spherical volume of radius a. Most antennas, however, are not spherically shaped for various reasons including ease of fabrication and conformality to the structures that they are mounted on. Therefore, most electrically-small antennas do not efficiently utilize the volume within the Chu's sphere and thus, the fundamental limits that govern their performances is not accurately predicted by the Chu limit. Additionally, many small ultra-wideband antennas are multi-resonant structures and the Chu limit does not directly apply to them. In [34], Gustafsson *et al.* proposed a method for determining the fundamental limits on the performances of electrically-small antennas, which takes the general form factor of the antenna into account. In [30] Sohl and Gustafsson presented a similar method that examines the fundamental limits on the performances of compact, ultra-wideband antennas. This analysis takes into account the tradeoffs between the operating frequency band, form factor, size, and the partial realized gain of the antenna. The study presented in [30] is one of the most rigorous published studies that quantify the fundamental limits on the performances of compact UWB antennas. In this section, we compare the performance of the proposed antenna against the Sohl-Gustafsson fundamental limitations on UWB antennas discussed in [30].

Consider an antenna with an arbitrary shape as a scatterer, placed in free space and subject to the excitation of an incident plane wave. The antenna's realized gain must satisfy [30]:

$$\int_0^\infty \frac{g(k;\hat{\boldsymbol{k}},\hat{\boldsymbol{e}})}{k^4}dk = \frac{\eta}{2}(\hat{\boldsymbol{e}}\cdot\boldsymbol{\gamma_e}\cdot\hat{\boldsymbol{e}} + (\hat{\boldsymbol{k}}\times\hat{\boldsymbol{e}})\cdot\boldsymbol{\gamma_m}\cdot(\hat{\boldsymbol{k}}\times\hat{\boldsymbol{e}})) \quad (3)$$

where $g(k;\hat{\boldsymbol{k}},\hat{\boldsymbol{e}})$ is the realized gain of the antenna in the $\hat{\boldsymbol{k}}$ direction with respect to the $\hat{\boldsymbol{e}}$ polarization, k is the wavenumber in free space, η is the absorbtion efficiency, and $\boldsymbol{\gamma_e}$ and $\boldsymbol{\gamma_m}$ are the electric and magnetic polarizability dyadics, respectively. In this method [30], the antenna is considered as a scatterer placed in free space. Absorbtion efficiency is defined as the efficiency of power absorbed by the scatterer which is excited by an incident plane wave. Polarizability dyadic is a 3×3 rank tensor. Each element in the matrix describes the response parallel or perpendicular to the direction of the incident field. The detailed derivation is given in the Appendix of [34]. This equation is valid for antennas having an arbitrary geometry and including electric and magnetic materials. If the material properties are not considered, we can introduce the high-contrast dyadic, $\boldsymbol{\gamma}_\infty$, defined as the limit of either $\boldsymbol{\gamma_e}$ or $\boldsymbol{\gamma_m}$ when the electric or magnetic susceptibility dyadic becomes infinitely large in the volume circumscribing the antenna [34]:

$$\begin{aligned}\hat{\boldsymbol{e}}\cdot\boldsymbol{\gamma}_\infty\cdot\hat{\boldsymbol{e}} &\geqslant \hat{\boldsymbol{e}}\cdot\boldsymbol{\gamma_e}\cdot\hat{\boldsymbol{e}},\\ (\hat{\boldsymbol{k}}\times\hat{\boldsymbol{e}})\cdot\boldsymbol{\gamma}_\infty\cdot(\hat{\boldsymbol{k}}\times\hat{\boldsymbol{e}}) &\geqslant (\hat{\boldsymbol{k}}\times\hat{\boldsymbol{e}})\cdot\boldsymbol{\gamma_m}\cdot(\hat{\boldsymbol{k}}\times\hat{\boldsymbol{e}})\end{aligned} \quad (4)$$

In microwave regime, magnetic materials are usually not used in antennas due to their lossy characteristics and the lack of availability of magnetic materials operating at frequencies beyond a few hundred megahertz. Therefore, only $\boldsymbol{\gamma_e}$ is required to be considered for most cases as well as the case examined in this work. Assuming $\boldsymbol{\gamma_m}$ is 0, (3) can be simplified as,

$$\int_0^\infty \frac{g(k)}{k^4}dk \leqslant \frac{\eta\gamma}{2} \quad (5)$$

where $\gamma = \hat{\boldsymbol{e}}\cdot\boldsymbol{\gamma}_\infty\cdot\hat{\boldsymbol{e}}$. The method for calculating $\boldsymbol{\gamma}_\infty$ for an antenna is described in detail in [35].

This article has been accepted for publication in a future issue of this journal, but has not been fully edited. Content may change prior to final publication. Citation information: DOI 10.1109/TAP.2016.2641925, IEEE Transactions on Antennas and Propagation

TABLE I
PHYSICAL DIMENSIONS OF THE PROPOSED ANTENNA.

Parameter	W_1	W_2	W_3	W_4	W_5	W_6	f_l	f_w	g
Value (mm)	2	41.3	20	1	30	2	37	2	1
Parameter	L_1	L_2	L_3	L_4	L_5	M_1	M_2	D	H
Value (mm)	38	27.5	18.1	13.7	30	3	0.35	62.6	39

Next, we consider the case of a hypothetical vertically polarized, omni-directional antenna that fits within a cylindrically-shaped volume having a height of l and a diameter of d, as shown in Fig. 6(a). The height-to-diameter ratio is defined as $\xi = l/d$. This cylindrical volume is confined in the Chu's sphere with radius of a. We make a number of assumptions about this hypothetical antenna. These include: (i) The antenna is well matched (i.e., $\eta = 1/2$); (ii) The antenna bandwidth is 4.1:1 (i.e., the same as the bandwidth of the proposed antenna shown in Fig. 1); and (iii) At each frequency within this bandwidth, the antenna has a gain similar to that of an ideal dipole with a physical length of l. With these assumptions, we use (3), (5) to determine the lowest possible $k_{min}a$ value for this UWB antenna.

Applying (5), a_{min} can be found as a function of the lowest operating frequency and ξ, as depicted in Fig. 7. Observe that a_{min} increases as the lowest operating frequency decreases. This is very intuitive, since decreasing the lowest frequency of operation of the antenna requires increasing the size of the structure. In addition, for any specific lowest operating frequency, the optimized ξ value, resulting in the smallest a_{min}, is always 1.26. This is because ξ is only related to γ_∞, which itself only depends on the cylindrical volume's form. The boundary line corresponding $a_{min} = 50$ mm is plotted on the curved surface of Fig. 7. The portion of the surface for which $a_{min} \leqslant 50\ mm$ is on the left hand side of the line. This portion of the surface identifies the possible lowest frequencies of operation that can be obtained from the hypothetical antenna shown in Fig. 6(a) for any given height to width ratio satisfying the condition of $a_{min} < 50\ mm$. The optimized point in the available area that offers the minimum lowest frequency of operation of the antenna can be found on this line. This point corresponds to a ξ value of 1.26, and the corresponding lowest operating frequency is 644 MHz. This means that the minimum value of the lowest operating frequency that can be expected from the aforementioned hypothetical UWB antenna, which fits in a sphere with $a = 50$ mm is 644 MHz.

B. Designing the Proposed UWB Antenna to Approach the Fundamental Limits

The hypothetical UWB antenna studied in the previous section has many of the attributes of the antenna proposed in this work. These include omni-directionality, dipole (or monopole) like radiation patterns with vertical polarization, 4.1:1 impedance bandwidth with a low VSWR, and a cylindrical form factor. Based on the study of the previous sub-section, it can be concluded that the height-to-diameter ratio, ξ, is a crucial parameter to describe the antenna's form factor. A small ξ means the cylinder is like a planar circular disk while a large ξ means the cylinder is like a thin wire. Both scenarios produce smaller polarizability dyadics, thereby leading to increasing the lowest frequency of operation for a fixed value of a. Since the optimized value of ξ is 1.26 as described in the previous sub-section, the corresponding dimensions of the proposed antenna are $H = 39\ mm$ and $D = 62.6\ mm$, which satisfy $\xi \simeq 1.26$ and $a = 50\ mm$. Detailed physical dimensions of the proposed antenna are summarized in Table I.

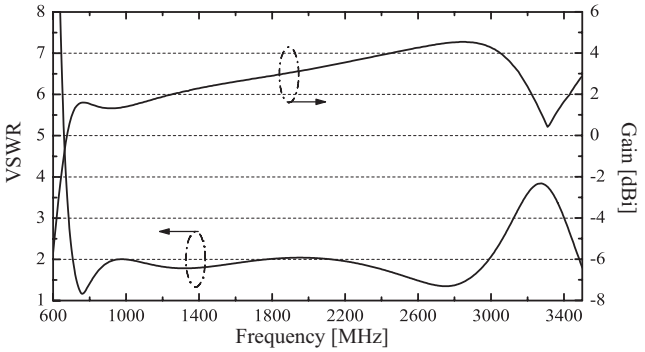

Fig. 8. Simulated VSWR and realized gain of the dipole version of the proposed antenna shown in Fig. 6(b).

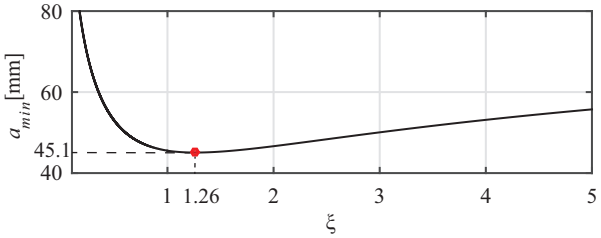

Fig. 9. Minimum required a (a_{min}) as a function of the height-to-diameter ratio, ξ, for the dipole version of the proposed antenna shown in Fig. 6(b).

The ground plane of the antenna examined in Section III was considered to be infinite. Therefore, to obtain the Sohl-Gustafsson theoretical limit for this antenna, the antenna's ground plane is removed and the image of the radiator shown in Fig. 1(c) is built and connected to the original radiator, as shown in Fig. 6(b). Because of the differences between the input impedances of the monopole and dipole versions of the proposed antenna, the characteristic impedance of the two feed ports is doubled to 200 Ω. These changes ensure that the antenna with two mirrored radiators shown in Fig. 6(b) can fit in the cylindrically-shaped volume and has the same performance and input impedance response as that of the proposed antenna shown in Fig. 2(g). Fig. 8 shows the simulated VSWR and gain of this antenna. The antenna has an impedance bandwidth of 4.24:1 spanning the frequency range of 702-2990 MHz, which is very similar to its monopole version. Due to the absence of the ground plane, the maximum antenna gain is reduced by ∼2.5 dBi as compared to the monopole version. Using these simulation results in (5), the a_{min} from the antenna can be obtained, as shown in Fig. 9. Observe that the optimized value of ξ is still 1.26, and the corresponding a_{min} is 45.1 mm. This means that, theoretically, an optimum UWB antenna with a lowest frequency of operation of 702 MHz, an impedance bandwidth of 4.24:1,

This article has been accepted for publication in a future issue of this journal, but has not been fully edited. Content may change prior to final publication. Citation information: DOI 10.1109/TAP.2016.2641925, IEEE Transactions on Antennas and Propagation

and a realized gain similar to that shown in Fig. 8 must have a maximum linear dimension larger than 2 × 45.1 mm (i.e., $a_{min} = 45.1\ mm$). In the present design, these attributes are obtained from an antenna with $a = 50\ mm$. Therefore, the ratio between a and a_{min} is ≈ 1.1. This demonstrates that, for its operating bandwidth, realized gain, and form factor, the antenna proposed in this work has an occupied volume that is only 10% larger than the theoretical limits predicted in [30]. Therefore, the proposed antenna has a nearly optimum performance. The results presented in this sub-section are also consistent with those presented in Section IV-A. Specifically, both results demonstrate that for the same form factor and frequency response, the antenna proposed in this work has a $k_{min}a$ value that is approximately 10% greater than the minimum achievable $k_{min}a$ value.

V. Fabrication and Measurement Results

Fig. 10 shows the photograph of the fabricated prototype of the proposed antenna. It was fabricated out of 10 mil-thick brass sheets. The fabricated antenna was mounted on a square-shaped aluminum plate as its ground plane, which has dimensions of 430 mm × 430 mm. The antenna feed network was fabricated on a 1.58-mm thick FR4 substrate. After taking the thickness of the brass sheets, the FR4 feed network, as well as the connecting wires between the antenna and the feed network into account in simulation, we found that the impedance matching of the proposed antenna was changed slightly. Therefore, the two 100 Ω branch lines of the microstrip feed network were replaced by 125 Ω lines (i.e., $M_2 = 0.35\ mm$) to obtain a better impedance matching in the fabricated prototype.

The input VSWR of the antenna was measured using an Agilent N5225A vector network analyzer and its radiation patterns and gain were measured using a spherical near field system (SATIMO StarLab E-18 GHz). The measured and simulated VSWRs and the realized gain of the antenna are plotted in Fig. 11. Measurement results show that the antenna provides a VSWR better than 2:1 over a 4.1:1 bandwidth covering the range of 693 to 2840 MHz. This lowest frequency of operation corresponds to a $k_{min}a = 0.726$. Measurement and simulation results are in general agreement with each other. Within the operating frequency range, the measured maximum realized gain increases with frequency and varies in the range of 3.8 to 7.5 dBi and the simulated gain varies between 3.3 and 7.2 dBi. As can be seen, a reasonable agreement between the simulation and measurement is achieved. The discrepancies observed between the simulation and measurement results are primarily attributed to the fabrication tolerances. Within the operating frequency band, the total efficiency of the proposed antenna (inclusive of the mismatch losses) remains above 80%. At the lowest frequency of operation of the antenna, the total efficiency is 84.5% and the corresponding radiation efficiency is extracted by taking out the effects of the impedance mismatch, and is found to be 95.1%.

Fig. 12 shows the measured and simulated radiation patterns of the antenna at four different frequencies of 700, 1100, 1700, and 2600 MHz within its operating band. The results

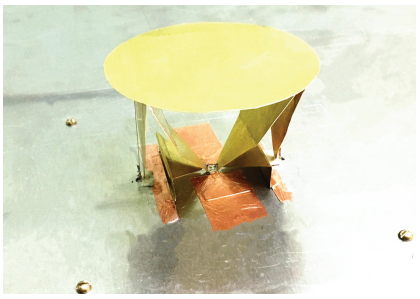

Fig. 10. Photograph of the antenna prototype.

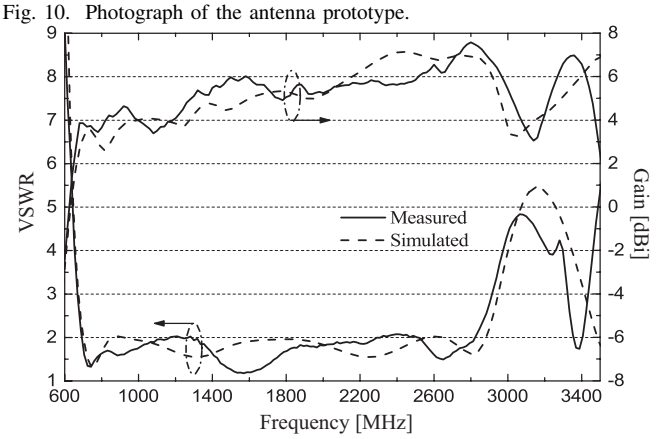

Fig. 11. Simulated and measured VSWRs and realized gains of the antenna.

are shown for two different elevation cuts (the $x-z$ and $y-z$ planes) and the azimuth plane (the $x-y$ plane). It can be seen that the proposed antenna exhibits good monopole-like radiation characteristic across its entire band of operation and despite not being rotationally symmetric by 90°, the elevation radiation patterns in the $x-z$ and $y-z$ planes are very similar. The measured cross-polarization radiation level is generally below -20 dB in the $x-z$ and $y-z$ planes. Since some of the simulated cross-polarized radiation patterns are lower than -40 dB, they are not illustrated on the graphs. However, in the azimuth plane (the $x-y$ plane), the measured cross-polarization level is higher and decreases with frequency from -4.5 dB to -13.5 dB. This higher level of cross polarization is due to the diffraction effects on the outer edges of the square-shaped ground plane with a finite size (i.e., $430\ mm \times 430\ mm$). The current density along the edges of the ground plane can be lowered by increasing the size of the ground plane or treating the edges with thin sheets of absorbers. This alleviates the diffraction effects and reduces the cross-polarization level. Alternatively, using a circular-shaped ground plane is another effective way to decrease the cross-polarization level. The surface currents on a circular-shaped ground plane have the same magnitude and phase when they reach at the edge of the ground plane. Each current flowing along the edge can find a counterpart to cancel out each other. Therefore, the diffraction effects on the edges of the circular-shaped ground plane are suppressed and the cross-polarization level can be reduced significantly. Fig. 13 shows the minimum cross-polarization discriminations of the radiation patterns in the $x-y$ plane, which is defined as

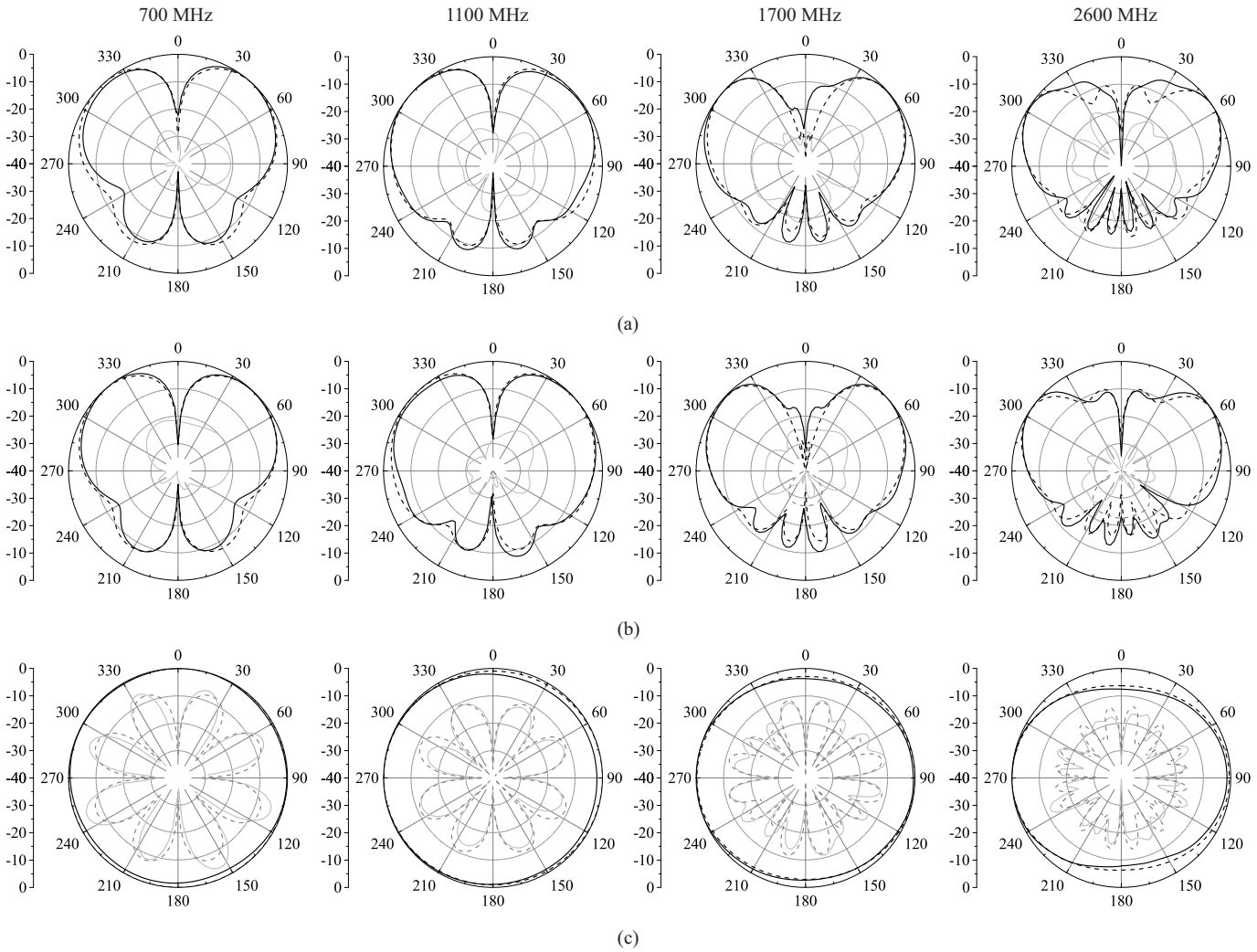

Fig. 12. Simulated and measured radiation patterns of the proposed antenna at 700, 1100, 1700 and 2600 MHz. The black solid line is the measured co-pol, the gray solid line is the measured cross-pol, the black dashed line is the simulated co-pol, the gray dashed line is the simulated cross-pol. (a) $x-z$ plane, (b) $y-z$ plane, and (c) $x-y$ plane.

the maximum co-polarization level over the maximum cross-polarization level of the radiation pattern in the $x-y$ plane. The proposed antenna with a circular-shaped ground plane has a much higher cross-polarization discrimination than that of the antenna with a square-shaped ground plane. Up to 38 dB enhancement can be achieved by using a circular-shaped ground plane. The difference between the discriminations of the two scenarios is decreased with frequency. This is due to the fact that, at the higher frequencies, the primary factor contributing to the cross-polarization is the antenna structure.

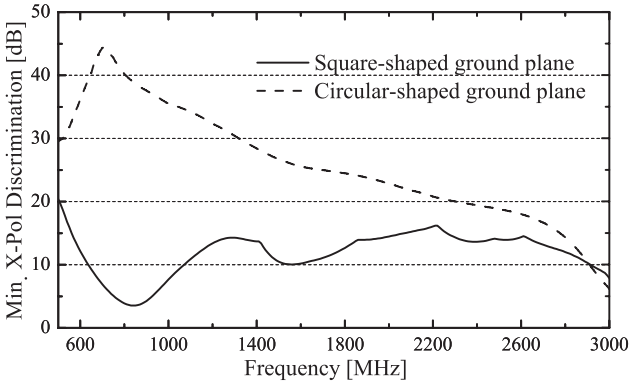

Fig. 13. Minimum cross-polarization discrimination of the radiation patterns of the proposed antenna with the square- or circular-shaped ground planes in the azimuth plane.

VI. Further Antenna Miniaturization and Comparison with the State-of-the-Art

Further reduction of the $k_{min}a$ value of the proposed antenna is possible by utilizing the volume available within the Chu's sphere more efficiently. This expectation is justified by examining (3) and observing that a sphere has the largest polarizability dyadic (i.e., $4\pi a^3$) compared with other shapes. Therefore, to further reduce the lowest frequency of operation of the antenna, without increasing its maximum linear dimension, the planar circular top hat of the antenna is replaced by a spherical top one. The radius of the sphere, a, is maintained at 50 mm to allow for a fair comparison with the previous

This article has been accepted for publication in a future issue of this journal, but has not been fully edited. Content may change prior to final publication. Citation information: DOI 10.1109/TAP.2016.2641925, IEEE Transactions on Antennas and Propagation

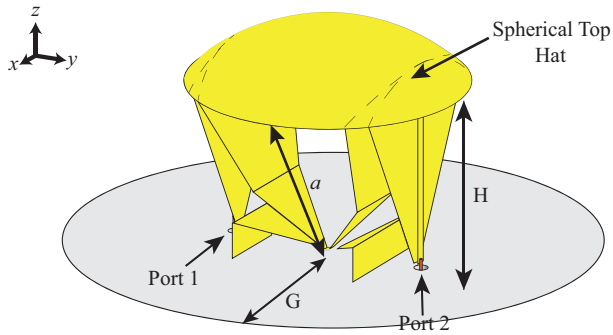

Fig. 14. Topology of the proposed antenna with a spherical top hat. Physical dimensions are: $W_1 = 2, W_2 = 58, W_3 = 34, W_4 = 1, W_5 = 30, W_6 = 2, L_1 = 28, L_2 = 12.4, L_3 = 23.6, L_4 = 6, L_5 = 10.3, f_l = 38.3, f_w = 2, g = 1, H = 29, G = 275$. All units are in [mm].

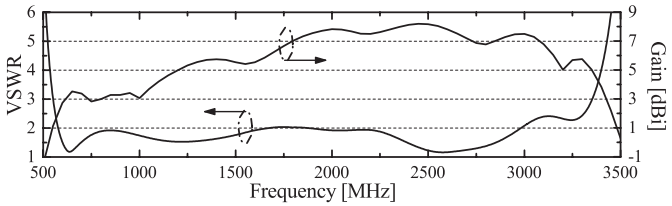

Fig. 15. Simulated VSWR and realized gain of antenna with spherical top hat.

design. This modification enables a more efficient utilization of the volume within Chu's sphere. To improve the impedance matching of the modified antenna, two shunt 70 nH inductors are added to the input terminals of each loop (ports 1 and 2 as shown in Fig. 1(d)). The topology of this antenna is shown in Fig. 14. All the relevant physical dimensions of the antenna are provided in the caption of Fig. 14.

Fig. 15 shows the simulated VSWR and realized gain of this antenna. The antenna has the same maximum linear dimension as the structure discussed in the previous section but provides a wider bandwidth and operates at lower frequencies. It has a VSWR better than 2:1 and a bandwidth covering the range of 576 to 2985 MHz (5.2:1 bandwidth). The lowest frequency of operation of this antenna corresponds to a $k_{min}a = 0.6$. Within the operating frequency range, the maximum realized gain increases with frequency and varies in the range of 2 to 8.1 dBi. At the lowest frequency of operation of the antenna, the simulated radiation efficiency is 85.1%. In addition, the antenna exhibits good monopole-like radiation characteristic across its entire band of operation with radiation patterns similar to the one shown in Fig. 12.

The proposed designs are compared with a few other prominent compact, UWB or wideband antenna examples reported in the literature and the results are presented in Table II. The antennas included in this comparison are all structures that have compact dimensions and radiate vertically-polarized waves with omni-directional radiation patterns (similar to a monopole antenna). Compared with other designs, the proposed antenna with a planar top hat has a small $k_{min}a$ value, which is equal to the $k_{min}a$ value of the Goubau antenna. However, the proposed antenna offers a significantly wider bandwidth compared to Goubau's antenna. This is due to the fact that, while both antennas have the same maximum linear dimensions ($a = 0.115\lambda_{min}$), the proposed antenna has the optimum height-to-diameter radio as discussed in Section IV-A and the height-to-diameter raio of the Goubau's antenna is not optimum. Indeed the height-to-width ratio of the Goubau's antenna is 0.70, which is different from the optimum ξ value derived in Section III. Therefore, the proposed antenna utilizes the volume within Chu's sphere more efficiently. As can be observed from Table II, the spherical version of the proposed antenna has the lowest $k_{min}a$ value among the UWB antennas (i.e., antennas providing at least 50% bandwidth or more) reported in Table II. To the best of our knowledge, this is the first design that reports such a combination of ultra-wide bandwidth and low $k_{min}a$ and this combination of bandwidth and low $k_{min}a$ values of the proposed antennas have not been previously achieved.

VII. Conclusions

A compact, ultra-wideband, capacitively-fed antenna design having either a cylindrical or spherical form factor was presented. The proposed antenna takes advantage of two three-dimensional split loops as the main radiator, a circular top hat as the capacitive loading, and two strip-shaped probes as the antenna feeds to achieve UWB operation in a small occupied volume. The antenna has monopole-like radiation characteristics across its entire band of operation. The simulated performance of the proposed UWB antenna with a cylindrical form factor was also compared against the Sohl-Gustafsson theoretical limits on the performance of ultra-wideband antennas [30] and the form factor and general dimensions of the antenna were optimized to obtain a near optimum performance. Specifically, it was demonstrated that, at its lowest frequency of operation, the optimized version of the proposed antenna has a $k_{min}a$ value that is only 10% higher than the theoretical limits. A prototype of this antenna was fabricated and experimentally characterized. Experimental results demonstrated the validity of the theoretical predictions and were in good agreement with the simulation results. The fabricated prototype has dimensions of $R \times H = 0.072\lambda_{min} \times 0.09\lambda_{min}$ corresponding to a $k_{min}a$ = 0.73 and demonstrates a VSWR lower than 2 and a consistent omni-directional radiation pattern across a frequency band from 693-2840 MHz (4.1:1 ratio). A spherical version of the proposed antenna was also studied and demonstrated to offer an additional 18% miniaturization without increasing its maximum linear dimension. This design was shown to be capable of offering a VSWR lower than 2 over a 5.2:1 bandwidth with a $k_{min}a$ value of 0.60. To the best of our knowledge, the combination of ultra-wide bandwidth and the low $k_{min}a$ value of the proposed antenna is not matched by any other UWB antenna - that radiates in a monopole-like fashion - reported to date.

References

[1] G. Adamiuk, T. Zwick, and W. Wiesbeck, "UWB antennas for communication systems," *Proc. IEEE*, vol. 100, no. 7, pp. 2308–2321, Jul. 2012.

TABLE II
COMPARISON OF THE PERFORMANCE OF THE PROPOSED UWB ANTENNA WITH A NUMBER OF STATE-OF-THE-ART UWB AND WIDEBAND ANTENNAS REPORTED IN THE LITERATURE.

Ref.	Structure Type	Lumped Element Matching	Dimensions[1] (λ_{min}[2])	Operation Band[3](MHz)	Bandwidth[3]	Gain (dBi)	Radiation Efficiency	k_{min}[4] a
[9]	Sphere	No	$R = 0.078$	258-302	18%	n/a	>90%	0.49
[15]	Cube	No	$L \times W \times H = 0.015 \times 0.248 \times 0.248$	2950-11600	3.9:1	n/a	>79%	1.10
[17]	Cylinder	No	$R \times H = 0.096 \times 0.067$	466-916	1.9:1	n/a	n/a	0.73
[20]	Cylinder	Yes	$R \times H = 0.113 \times 0.079$	550-1635	3.0:1	n/a	>90%	0.87
[22]	Cube	No	$L \times W \times H = 0.2 \times 0.2 \times 0.06$	300-460	1.5:1	>1.9	n/a	0.97
[23]	Cylinder	No	$R \times H = 0.072 \times 0.143$	2150-14000	6.5:1	>0	n/a	1.01
[24]	Sphere	No	$R = 0.125$	2140-10000	4.7:1	n/a	n/a	0.79
[25]	Cube	No	$L \times W \times H = 0.204 \times 0.204 \times 0.087$	3060-12000	3.9:1	n/a	>95%	1.06
[27]	Cylinder	Yes	$R \times H = 0.095 \times 0.085$	600-3200	5.5:1	>2.1	>60%	0.80
[29]	Cube	Yes	$L \times W \times H = 0.26 \times 0.26 \times 0.046$	660-5600	8.5:1	>4	>70%	1.19
Circular top	Cylinder	No	$R \times H = 0.072 \times 0.09$	693-2840	4.1:1	>3.8	>95%	0.73
Spherical top	Sphere	Yes	$R = 0.096$	576-2985	5.2:1	>2	>85%	0.60

[1] R and H are the radius and the height, respectively, of the antennas that have a cylindrical form factor. L, W, and H are the length, width, and height, respectively, of the antennas that ave a rectangular box form factor. R is the radius of the antennas that have a spherical or semi-spherical form factor.
[2] λ_{min} is the free-space wavelength at the lowest frequency.
[3] VSWR is less than 2.
[4] k_{min} is the wavenumber at the lowest frequency of operation of the antenna.

[2] "SB-v16 / sb-v35 vertical HF whip antennas". [Online]. Available: http://rf.harris.com/media/SB-V16-SB-V35_tcm26-9214.pdf. [Accessed: 10- May- 2016].

[3] H. Wheeler, "Fundamental limitations of small antennas," *Proc. IRE*, vol. 35, no. 12, pp. 1479–1484, Dec. 1947.

[4] L. J. Chu, "Physical limitations of omni-directional antennas," *J. Appl. Phys.*, vol. 19, no. 12, pp. 1163–1175, 1948.

[5] D. Sievenpiper, D. Dawson, M. Jacob, T. Kanar, S. Kim, J. Long, and R. Quarfoth, "Experimental validation of performance limits and design guidelines for small antennas," *IEEE Trans. Antennas Propag.*, vol. 60, no. 1, pp. 8–19, Jan. 2012.

[6] K. Noguchi, S. Betsudan, T. Katagi, and M. Mizusawa, "A compact broad-band helical antenna with two-wire helix," *IEEE Trans. Antennas Propag.*, vol. 51, no. 9, pp. 2176–2181, Sep. 2003.

[7] S. Best, "Low Q electrically small linear and elliptical polarized spherical dipole antennas," *IEEE Trans. Antennas Propag.*, vol. 53, no. 3, pp. 1047–1053, Mar. 2005.

[8] O. Kim, "Low-Q electrically small spherical magnetic dipole antennas," *IEEE Trans. Antennas Propag.*, vol. 58, no. 7, pp. 2210–2217, Jul. 2010.

[9] H. Stuart and S. Best, "A small wideband multimode antenna," in *Proc. IEEE Antennas and Propag. Soc. Int. Symp.*, July 2008, pp. 1–4.

[10] W. Hong and K. Sarabandi, "Low-profile, multi-element, miniaturized monopole antenna," *IEEE Trans. Antennas Propag.*, vol. 57, no. 1, pp. 72–80, Jan. 2009.

[11] J. Oh, J. Choi, F. T. Dagefu, and K. Sarabandi, "Extremely small two-element monopole antenna for HF band applications," *IEEE Trans. Antennas Propag.*, vol. 61, no. 6, pp. 2991–2999, Jun. 2013.

[12] A. Erentok and R. Ziolkowski, "Metamaterial-inspired efficient electrically small antennas," *IEEE Trans. Antennas Propag.*, vol. 56, no. 3, pp. 691–707, Mar. 2008.

[13] M. Lee, K. Luk, K. Leung, and M. Leung, "A small dielectric resonator antenna," *IEEE Trans. Antennas Propag.*, vol. 50, no. 10, pp. 1485–1487, Oct. 2002.

[14] J. Liang, C. C. Chiau, X Chen and C. G. Parini, "Study of a printed circular disc monopole antenna for UWB systems," *IEEE Trans. Antennas Propag.*, vol. 53, no. 11, pp. 3500–3504, Nov. 2005.

[15] Z. N. Chen, T. S. P. See and X. Qing, "Small printed ultrawideband antenna with reduced ground plane effect," *IEEE Trans. Antennas Propag.*, vol. 55, no. 2, pp. 383–388, Feb. 2007.

[16] T. Dissanayake and K. P. Esselle, "Prediction of the notch frequency of slot loaded printed UWB antennas," *IEEE Trans. Antennas Propag.*, vol. 55, no. 11, pp. 3320–3325, Nov. 2007.

[17] G. Goubau, N. Puri, and F. Schwering, "Diakoptic theory for multi-element antennas," *IEEE Trans. Antennas Propag.*, vol. 30, no. 1, pp. 15–26, Jan. 1982.

[18] C. Friedman, "Wide-band matching of a small disk-loaded monopole," *IEEE Trans. Antennas Propag.*, vol. 33, no. 10, pp. 1142–1148, Oct. 1985.

[19] C. Ravipati and C. Reddy, "Low profile disk and sleeve loaded monopole antennas," in *Proc. IEEE Antennas and Propag. Soc. Int. Symp.*, vol. 2A, Jul. 2005, pp. 160–163.

[20] S. R. Best, "Progress in the design of a small wideband antenna," in *Proc. 30^{th} Antenna Appl. Symp.*, September 2006.

[21] H. Nakano, M. Takeuchi, and J. Yamauchi, "Hyper-wideband four-arm antenna," in *Proc. Int. Symp. on Antennas and Propag.*, Nov. 2015.

[22] J. Oh and K. Sarabandi, "Low profile vertically polarized omnidirectional wideband antenna with capacitively coupled parasitic elements," *IEEE Trans. Antennas Propag.*, vol. 62, no. 2, pp. 977–982, Feb. 2014.

[23] H. Nakano, H. Iwaoka, K. Morishita, and J. Yamauchi, "A wideband low-profile antenna composed of a conducting body of revolution and a shorted parasitic ring," *IEEE Trans. Antennas Propag.*, vol. 56, no. 4, pp. 1187–1192, Apr. 2008.

[24] T. Yang, W. A. Davis, and W. L. Stutzman, "The design of ultra-wideband antennas with performance close to the fundamental limit," Virginia Tech Antenna Group, Blacksburg, VA, USA, Tech. Rep., 2008.

[25] M. Koohestani, J.-F. Zurcher, A. Moreira, and A. Skrivervik, "A novel, low-profile, vertically-polarized UWB antenna for WBAN," *IEEE Trans. Antennas Propag.*, vol. 62, no. 4, pp. 1888–1894, Apr. 2014.

[26] J. Zhao, D. Psychoudakis, C.-C. Chen, and J. Volakis, "Design optimization of a low-profile uwb body-of-revolution monopole antenna," *IEEE Trans. Antennas Propag.*, vol. 60, no. 12, pp. 5578–5586, Dec 2012.

[27] S. Abadi and N. Behdad, "An electrically small, vertically polarized ultrawideband antenna with monopole-like radiation characteristics," *IEEE Antennas Wireless Propag. Lett.*, vol. 13, pp. 742–745, 2014.

[28] N. Behdad, M. Li, and Y. Yusuf, "A very low-profile, omnidirectional, ultrawideband antenna," *IEEE Antennas Wireless Propag. Lett.*, vol. 12, pp. 280–283, 2013.

[29] K. Ghaemi and N. Behdad, "A low-profile, vertically polarized ultra-wideband antenna with monopole-like radiation characteristics," *IEEE Trans. Antennas Propag.*, vol. 63, no. 8, pp. 3699–3705, Aug. 2015.

[30] C. Sohl and M. Gustafsson, "A priori estimates on the partial realized gain of ultra-wideband (UWB) antennas," *Q. J. Mech. Appl. Math.*, vol. 61, no. 3, pp. 415–430, 2008.

[31] B. S. W. R. Eisenstadt and B. M. Thompson, *Microwave Differential Circuit Design Using Mixed-Mode S-Parameters.* Boston, MA: Artech House, 2006.

[32] N. Behdad and K. Sarabandi, "A compact antenna for ultrawide-band applications," *IEEE Trans. Antennas Propag.*, vol. 53, no. 7, pp. 2185–2192, July 2005.

[33] K. Luk, C. Mak, Y. Chow, and K. Lee, "Broadband microstrip patch antenna," *Electronics Letters*, vol. 34, pp. 1442–1443(1), July 1998.
[34] M. Gustafsson, C. Sohl, and G. Kristensson, "Illustrations of new physical bounds on linearly polarized antennas," *IEEE Trans. Antennas Propag.*, vol. 57, no. 5, pp. 1319–1327, May 2009.
[35] M. Gustafsson, "Polarizability and physical bounds on antennas in cylindrical and rectangular geometries," Tech. Rep. TEAT-7195, 2010.

Mingjian Li (S'10-M'15) received the B.Sc. (Eng.) and Ph.D. degrees in electronic engineering from City University of Hong Kong in 2010 and 2014, respectively.

Currently, he is a post-doctoral research fellow with the Department of Electrical and Computer Engineering in the University of Wisconsin-Madison. His recent research interests include electrically small antennas, antenna characteristic modes, direction finding systems, millimeter-wave antennas and arrays, base station antennas, and circularly-polarized antennas. Dr. Li has served as a reviewer for over 15 scientific journals including *IEEE Transactions on Antennas and Propagation*. He received the Honorable Mention at the student contest of 2011 IEEE APS-URSI Conference and Exhibition. He was awarded the Best Student Paper Award in the 2012 IEEE International Workshop on Electromagnetics.

Nader Behdad (S'98-M'06-SM'12-F'17) received the B.S. degree in Electrical Engineering from Sharif University of Technology (Tehran, Iran) in 2000 and the M.S. and Ph.D. degrees in Electrical Engineering from University of Michigan - Ann Arbor in 2003 and 2006, respectively. Currently he is an Associate Professor in the Department of Electrical and Computer Engineering and the Harvey D. Spangler Faculty Scholar in the College of Engineering of the University of Wisconsin-Madison. From 2009-2013 he was an Assistant Professor in the Department of Electrical and Computer Engineering of the University of Wisconsin and from 2006 to 2008, he was as an Assistant Professor in the Department of Electrical Engineering and Computer Science of the University of Central Florida in Orlando, FL. Dr. Behdad's research expertise is in the area of applied electromagnetics. In particular, his research interests include electrically-small antennas, antenna arrays, antennas for biomedical applications, biomedical applications of RF/microwaves, periodic structures, frequency selective surfaces, passive high-power microwave devices, metamaterials, and biomimetics and biologically inspired systems in electromagnetics.

Dr. Behdad was named the Harvey D. Spangler Faculty Scholar by the College of Engineering (2016-2019) and the H. I. Romnes Faculty Fellow (2016-2021) by the Office of Vice Chancellor for Research and Graduate Education (OVCRGE) of the University of Wisconsin. He is the recipient of the ECE Rising Star Alumni Award from the University of Michigan in 2016, the Vilas Associates Award from the OVCRGE of UW-Madison in 2016, the 2014 R. W. P. King Prize Paper Award, and the 2012 Piergiorgio L. E. Uslenghi Letters Prize Paper Award of the IEEE Antennas and Propagation Society. In 2011, he received the CAREER award from the U.S. National Science Foundation, the Young Investigator Award from the United States Air Force Office of Scientific Research, and the Young Investigator Award from the United States Office of Naval Research. Prior to 2009, he received five different fellowships and awards from the Office of Naval Research, the International Union of Radio Science (URSI), and the University of Michigan-Ann Arbor among others. His graduate students were the recipients of the ten different awards/recognitions at the IEEE Pulsed Power & Plasma Science (2013), IEEE AP-S/URSI Symposium (2010, 2012, 2013, 2014, 2015), and the Antenna Applications Symposium (2008, 2010, 2011). Dr. Behdad served as the general co-chair of the 4th Arab-American Frontiers in Science, Engineering, and Medicine Symposium and as an Associate Editor for IEEE Antennas and Wireless Propagation Letters (2011-2015) and as the co-chair of the technical program committee of the 2012 IEEE International Symposium on Antennas and Propagation and USNC/URSI National Radio Science Meeting.